MATHEMATICAL MODELING AND COMPUTING, Vol. 10, No. 3, pp. 825–832 (2023)

A numerical 3D fluid-structure interaction model for blood flow in an atherosclerotic carotid artery

Kafi O.

CEMAT-Center for Computational and Stochastic Mathematics, University of Lisbon, Avenue Rovisco Pais 1049-001 Lisbon, Portugal

(Received 14 February 2023; Revised 20 July 2023; Accepted 26 July 2023)

Compelling evidence shows the association of inflammation with atherosclerosis diseases, one of the leading cause of mortality and morbidity worldwide. Recent research indicated that the inflammatory process of atherosclerotic lesions is involved in the progression of atherosclerotic plaques in specific regions, such as the carotid bifurcation, which represents a risk for ischemic stroke as a result of the interaction between the blood and the plaque. We start modeling using 3D idealized geometry in order to capture the most important features of such interactions. Then, we proceed to a partly patient-specific computational domain representing an atherosclerotic artery. Understanding such interactions is of paramount importance preventing the risk of the plaque rupture. The numerical results comparisons have shown that, qualitatively, there is an agreement between idealized atherosclerotic artery and patient-specific atherosclerotic carotid artery. The idealized carotid geometry will be useful in future FSI studies of hemodynamic indicators based on medical images.

Keywords: *atherosclerosis; blood flow; carotid bifurcation; fluid–structure interaction (FSI).*

2010 MSC: 74F10, 92C50, 97M60 **DOI:** 10.23939/mmc2023.03.825

1. Introduction

The inflammatory process of atherosclerosis leads to the formation of an atheromatous plaque in the intima of the blood vessel. It starts typically with the penetration of the low density lipoproteins (LDL) into the intima layer of the blood vessel where they are oxidized (ox-LDL). Being a dangerous agent, the ox-LDL triggers an immune response that initiates with the recruitment of monocytes, which are later transformed into macrophages. The macrophages eliminate the ox-LDL and are transformed into foam cells, that along with several other substances form the so-called lipid core. Smooth muscle cells migrate and form a fibrous cap which covers and isolates the lipid core from the blood circulation. The lipid core along with the fibrous cap constitute what is called the atheromatous plaque [1]. This process may occur throughout vessels in the body, however, there are regional differences in the susceptibility to lesion development. At the local level, susceptible sites for plaque formations are found at branch points of the vascular tree, such as the carotid bifurcation and in the lesser curvature of the aorta, where blood flow is characterized by low shear, oscillatory, and turbulent flow [2].

In this paper we will analyze some hemodynamic factors that have an important effect in the development and the risk rupture of atherosclerotic plaque in the carotid artery using a 3D fluid-structure interaction (FSI) numerical modeling. The methods to describe the interaction between fluid and structure are of great importance to achieve accurate numerical simulations. These methods include among others, the level set method [3], the immersed boundary method [4, 5], the fictitious domain method [6, 7], the Fully Eulerian formulation [8, 9] and the Arbitrary Lagrangian Eulerian (ALE) approach [10–12]. In this paper we use the ALE method to simulate our FSI model.

It is known that the circulatory system can be seen as an infinite extremely complex network including the heart and blood vessels. Therefore, mathematical and computational modeling of blood

flow dynamics is a complex problem that requires simplifying assumptions of the physical properties and boundary conditions (BCs). Rather than modeling the entire circulatory system, based on full 3D models, which is beyond the capability of current computers, segments of the circulation are studied to reduce the computational time, requiring appropriate inflow and outflow BCs. One can find an attempt in [13–15], where, after a 2D and a 3D analytical study to prove the existence of a weak solution for incompressible non-Newtonian fluids with nonstandard BCs, the authors tested the model numerically by coupling it with a nonlinear hyper-elastic model for the arterial wall and the atheromatous plaque.

Mechanical effects such as wall shear stress (WSS), pressure forces and structural stress are the most important factors. It is well accepted that low WSS is associated with the formation of plaques, whereas high WSS may impose higher risk of plaque rupture. Also, structural stresses are known to significantly affect the plaque vulnerability due to its considerable contribution to the total mechanical load [16]. Therefore, WSS and structural stress play important roles in view of risk evolution of plaque rupture. Several computational fluid dynamics (CFD) approaches have been proposed for modeling blood flow. These can be based on idealized geometries, but also on patient-specific geometries taken from medical imaging modalities, such as magnetic resonance imaging (MRI). The present study aims to compare some results obtained in the 3D idealized geometry with those obtained recently within a partly patient-specific computational domain representing an atherosclerotic artery.

2. Methods

2.1. Geometry of the atherosclerotic blood vessel

Idealized geometry. The computational domain is shown in Figure 1.

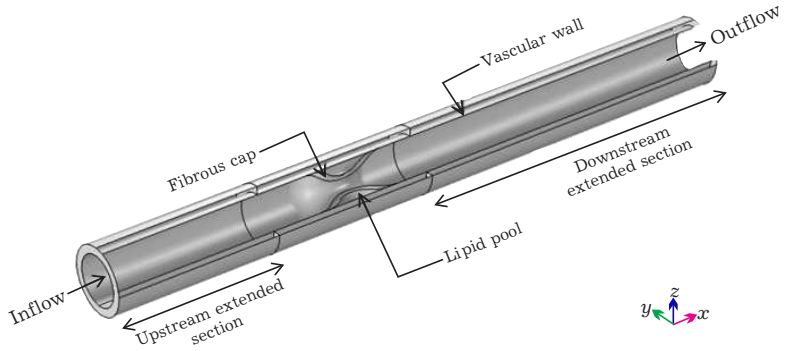

Fig. 1. 3D computational domain of the idealized stenosed artery model composed of fibrous cap, lipid pool and vascular wall.

It consists of a cylindrical tube representing the blood vessel with a narrowing of its interior to mimic the stenosis. The flow channel with radius $R = 0.3$ cm and height $H = 2$ cm contains the fibrous cap and lipid pool described by the trigonometric functions corresponding to a stenosis length of $l = 1$ cm. The degree of arterial stenosis is $\approx 70\%$ with a fibrous cap thickness of 0.5 mm. The thickness of the whole wall was chosen to be 1 mm. To avoid the entrance and exit effects, the computational domain was extended upstream (2 cm) and downstream (4 cm) the stenosis.

Reconstructed geometry. Our image-based modeling approach involves the following steps. First, the geometry of the stenotic carotid artery that will be used in our simulations is derived from MRI (see Figure 2(a)). To construct such geometry, several free computational tools are available, such as ITK-SNAP, SimVascular or 3DSlicer. Also commercial options such as Simpleware Scan IP, may be used. This geometry consists of the lumen, that is the interior of the artery. Moreover, the branches were extended to avoid the entrance and exit effects (see Figure 2(b)). Finally, the last realistic geometry was obtained in MeshLab in order to repair and smooth the model surface. Then, in order to design the FSI model, an open-source tool obtained from the finite element library LifeV developed in Politecnico di Milano [18] was used to generate the wall from the vessel lumen surface model previously obtained (see Figure 2(c)).

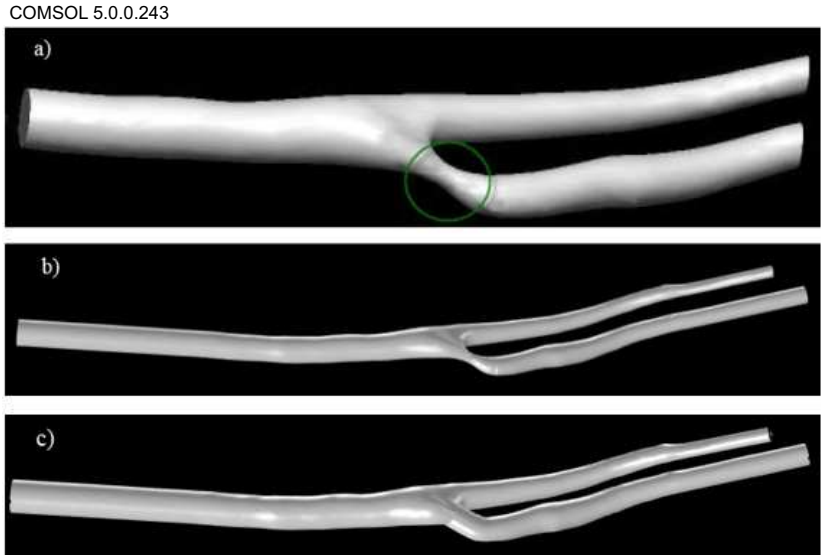

Fig. 2. (a) Medical image of the lumen of a carotid bifurcation with a stenotic region [17]. (b) The extended lumen. (c) Computational domain after fibrous cap, lipid pool and vascular wall construction.

2.2. Fluid–structure interaction modeling

Fluid modeling. As we are dealing with arteries with sufficiently large diameters, here we consider blood as an incompressible fluid, described by the quasi-Newtonian equations for the conservation of mass and linear momentum, as follows:

$$\begin{aligned} \rho_f \frac{\partial \mathbf{u}}{\partial t} + \rho_f(\mathbf{u}\cdot\nabla)\mathbf{u} - \nabla\cdot(2\mu(\mathbf{s}(\mathbf{u}))\mathbf{D}\mathbf{u}) + \nabla p = 0, \\ \nabla\cdot\mathbf{u} = 0. \end{aligned} \tag{1}$$

This system of time dependent partial differential equations involves the blood velocity $\mathbf{u} = [\mathbf{u}_1,\ \mathbf{u}_2,\ \mathbf{u}_3]^T$ and the pressure p as the unknown variables. The dynamic viscosity μ is a function of the strain rate tensor $\mathbf{D}\mathbf{u} = \frac{1}{2}(\nabla\mathbf{u} + (\nabla\mathbf{u})^T)$. More precisely, μ is a function of $\mathbf{s}(\mathbf{u})$, the second invariant of the strain rate tensor, defined by

$$(\mathbf{s}(\mathbf{u}))^2 = 2\mathbf{D}\mathbf{u} : \mathbf{D}\mathbf{u} = 2\sum_{i,j}(\mathbf{D}\mathbf{u})_{ij}(\mathbf{D}\mathbf{u})_{ji}.$$

We consider μ defined by the Carreau–Yasuda law,

$$\mu(\mathbf{s}(\mathbf{u})) = \mu_\infty + (\mu_0 - \mu_\infty)(1 + (\lambda\mathbf{s}(\mathbf{u}))^2)^{(n-1)/2},$$

with $\mu_0 = 0.0456$ Pa·s (the viscosity at the lowest shear rate), and $\mu_\infty = 0.0032$ Pa·s (the viscosity at the highest shear rate), $\lambda = 10.03$ s, $\rho_f = 1060$ Kg·m^{-3} (the fluid density) and $n = 0.344$ (corresponding to a shear-thinning viscosity fluid). The values of these parameters are taken from [19]. Although for large and almost cylindrical vessels a constant viscosity may be considered, it has been shown that, for stenotic cases, the shear-thinning nature of blood should not be neglected, if one is interested in hemodynamic factors such as recirculation size and WSS magnitudes. See, for instance [20].

Artery wall and plaque structures modeling. Consider the 3D nonlinear model of hyperelasticity [21], governed by the equation

$$\rho_s \frac{\partial^2 \boldsymbol{\eta}}{\partial t^2} - \operatorname{div}(\mathbf{F}\mathbf{S}) = 0, \tag{2}$$

where $\boldsymbol{\eta}$ represents the displacement vector, $\mathbf{F}$ is the deformation gradient tensor, given by $\mathbf{F} = \mathbf{I}_3 + \nabla\boldsymbol{\eta}$ ($\mathbf{I}_3$ is the identity matrix), and $\mathbf{S}$ represents the second Piola–Kirchhoff stress tensor. $\mathbf{S}$ can be computed as $\mathbf{S} = \frac{\partial\omega}{\partial\boldsymbol{\varepsilon}}$ where the strain tensor $\boldsymbol{\varepsilon}$ is defined by

$$\boldsymbol{\varepsilon} = \frac{1}{2}\big(\nabla\boldsymbol{\eta} + (\nabla\boldsymbol{\eta})^T + (\nabla\boldsymbol{\eta})^T\nabla\boldsymbol{\eta}\big),$$

and ω is the elastic strain energy density, which is material dependent.

In this work we assume the vessel wall to be modeled as St Venant–Kirchhoff material. Under this assumption, $\mathbf{S}$ becomes defined by the stress-strain relationship

$$\mathbf{S} - \mathbf{S}_0 = \mathbf{C} : (\boldsymbol{\varepsilon} - \boldsymbol{\varepsilon}_0 - \boldsymbol{\varepsilon}_{inel}),$$

where $\mathbf{S}_0$ and $\boldsymbol{\varepsilon}_0$ represent the initial second Piola–Kirchhoff stress and strain tensors, respectively, $\boldsymbol{\varepsilon}_{inel}$ the inelastic strain tensor and $\mathbf{C}$ the fourth-order stiffness tensor. The symbol "**:**" stands for the inner product of two second-order tensors. Here, we neglect the effects of $\mathbf{S}_0$, $\boldsymbol{\varepsilon}_0$ and $\boldsymbol{\varepsilon}_{inel}$.

The vessel wall is considered isotropic in such a way that the stiffness tensor has no preferred direction and the corresponding tensor components are computed internally according to:

$$\mathbf{C}^{ijkl} = \lambda_s \boldsymbol{g}^{ij}\boldsymbol{g}^{kl} + \mu_s(\boldsymbol{g}^{ik}\boldsymbol{g}^{jl} + \boldsymbol{g}^{il}\boldsymbol{g}^{jk}),$$

where $\lambda_s = \frac{\nu E}{(1-2\nu)(1+\nu)}$ and $\mu_s = \frac{E}{2(1+\nu)}$ are the Lamé coefficients, E is the Young modulus ($E = 2 \cdot 10^6$ Pa), ν is the Poisson ratio ($\nu = 0.45$) and $\boldsymbol{g}$ the metric tensor. As a result, we could also express the stress in terms of the strain as $\mathbf{S} = \lambda_s \operatorname{tr}(\boldsymbol{\varepsilon})\mathbf{I}_3 + 2\mu_s\boldsymbol{\varepsilon}$.

Concerning the structural domain representing the atheromatous plaque, we assume that it behaves differently from the wall, specifically, to verify the so-called Mooney–Rivlin Hyperelastic assumption. According to this, the second Piola–Kirchhoff stress tensor is given by $\mathbf{S} = \frac{\partial \omega}{\partial \boldsymbol{\varepsilon}}$ with

$$\omega = C_{10}(\bar{I}_1 - 3) + C_{01}(\bar{I}_2 - 3) + \frac{1}{2}\kappa(\bar{J} - 1)^2. \tag{3}$$

In (3), $\bar{J}$ represents the ratio between the current and original volumes and $\bar{I}_1$, $\bar{I}_2$ are the first two modified strain invariants, to be independent of the volume change ($\bar{I}_1 = I_1/\bar{J}^{2/3}$ and $\bar{I}_2 = I_2/\bar{J}^{4/3}$, where I_1 and I_2 are the first two strain invariants). The use of these modified invariants and the last term in equation (3) allows the description of nearly incompressible materials.

Coupling and boundary conditions. To couple fluid and structures equations (1) and (2) we used an ALE formulation. We rewrite the equations of the fluid, the generalized Navier–Stokes equations, in the ALE formulation as

$$\rho_f \frac{\partial \mathbf{u}}{\partial t}\Big|_X + \rho_f((\mathbf{u} - \boldsymbol{w}) \cdot \nabla)\mathbf{u} - \nabla_x \cdot (2\mu(\mathbf{s}(\mathbf{u}))\mathbf{D}\mathbf{u}) + \nabla_x p = 0, \tag{4}$$

where X is the Lagrangian coordinate and x is the Eulerian coordinate. $\boldsymbol{w}$ is the domain velocity. If $\boldsymbol{w}$ is zero, the method is simply an Eulerian approach, otherwise, if $\boldsymbol{w}$ is equal to the velocity of the fluid then the approach is Lagrangian. $\boldsymbol{w}$ can vary arbitrarily and continuously from one value to another in the fluid field. Two coupling conditions were also considered at the blood-wall interface:

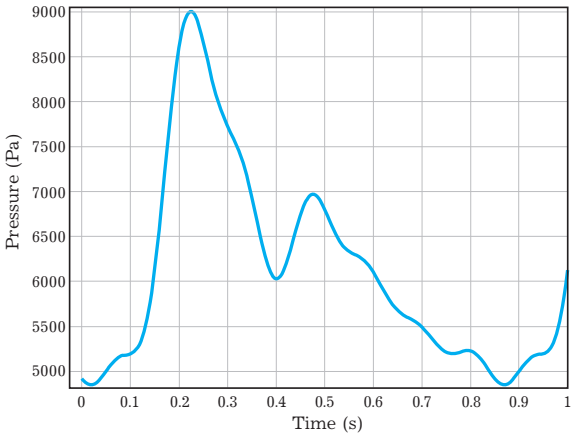

Fig. 3. Inlet pressure waveform.

- the continuity of the velocity in time

$$\mathbf{u} = \frac{\partial \boldsymbol{\eta}}{\partial t},$$

- and the equilibrium of the stresses

$$-\big(2\mu(\mathbf{s}(\mathbf{u}))\mathbf{D}\mathbf{u} - p\mathbf{I}_3\big)\mathbf{n} = J^{-1}\mathbf{F}\mathbf{S}\mathbf{F}\mathbf{n},$$

where $J = \det(\mathbf{F})$ and $\mathbf{n}$ is the outward unit vector to the solid domain. This condition should be rewritten on the interface at $t = 0$ to be prescribed on the structure model. Using the Piola transform we have

$$-J(2\mu(\mathbf{s}(\mathbf{u}))\mathbf{D}\mathbf{u} - p\mathbf{I}_3)\mathbf{F}^{-T}\mathbf{n}_0 = \mathbf{F}\mathbf{S}\mathbf{n}_0,$$

where $\mathbf{n}_0$ the outward unit vector to the interface at $t = 0$ (see [22]). The pressure waveform at the inlet is shown in Figure 3. In the following section, the simulations were performed over one cardiac cycle: 0.875 s (systolic and diastolic period).

At the outlets we consider typical natural BCs where we fix the stress

$$2\mu(\mathbf{s}(\mathbf{u}))\mathbf{D}\mathbf{u} \cdot \mathbf{n} - p\mathbf{n} = -\bar{p}\mathbf{n}, \tag{5}$$

$\bar{p} = \frac{\sqrt{\rho_f \beta}}{\sqrt{2}A_0^{5/4}}Q$, where Q is the flow rate and A_0 the cross-section reference area at rest. The coefficient β

is related to the mechanical properties of the vessel wall through the expression $\beta = \frac{\sqrt{\pi}h_0 E}{1-\nu^2}$, where E is the Young modulus, h_0 is the wall thickness and ν is the Poisson ratio. This linear absorbing condition (LAC) has a form of pressure, used in [23] and [24] to reduce significantly the spurious oscillations due to backflow from the outlets in a truncated geometrical domain.

3. Computational approach

The resulting coupled system of motion and fluid equations was solved using a finite element space discretization based on P1-P1 stabilized elements for the fluid, and P2 elements for the structure. The time discretization was based on the BDF of order 2, with a maximum time step of 5×10^{-3} s. The nonlinearities were tackled using Newton's method and each linear iteration solved with the direct PARDISO solver. The simulations were made using Comsol Multiphysics 5.0 in a workstation with a processor Dual CPU Xeon CPU E5-2630 v3 @ 2.4GHz and 128 GB RAM memory was used.

In order to improve the accuracy while minimizing the computational cost, we set different element sizes for the mesh approximating the 3D geometry. Therefore, we used smaller element sizes for the lipid pool and the fibrous cap, which are regions characterized by strong gradients and high stresses (see Figure 4).

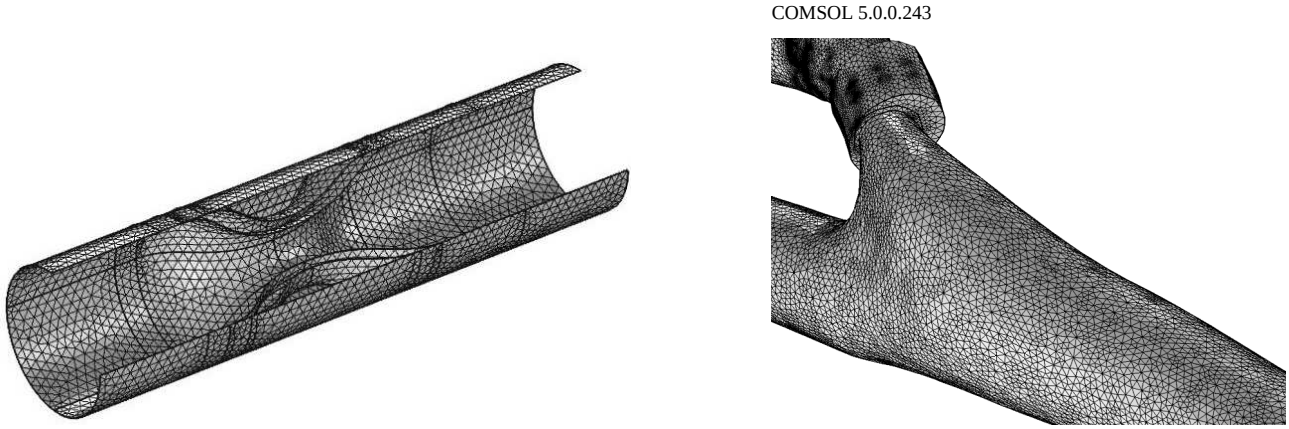

Fig. 4. Left: The 3D mesh for the idealized geometry. Right: The 3D mesh for the constructed athersclerotic carotid bifurcation.

All the computations and results presented in the next section were performed with the mesh that corresponds to a total number of degrees of freedom (DOF) of 3 826 996 for the realistic geometry and 449 048 DOF for the idealized one. Additional simulations using a coarse and an intermediate size mesh have been performed to analyze the convergence of the numerical solutions.

4. Numerical results

We performed a 3D FSI numerical simulations for blood flow in an idealized atherosclerotic artery then in a partly patient-specific atherosclerotic carotid bifurcation. We distinguish between the lipid pool and the fibrous cap by choosing the energy function parameter C_{10}, C_{01} and κ in agreement with experimental measurements taken from [25, 26] (Table 1).

Table 1. Parameters used for the plaque components.

Plaque components	C_{10} (N·m^{-2})	C_{01} (N·m^{-2})	κ (MPa)	Density (kg·m^{-3})
Fibrous cap	9200	0	3000	1000
Lipid pool	500	0	200	1000

We plot the results obtained in two geometries comparing three hemodynamic indicators: fluid velocity, total volume displacement and the WSS. This allows a simultaneous perception of the behavior of the atherosclerotic artery under these hemodynamic alterations.

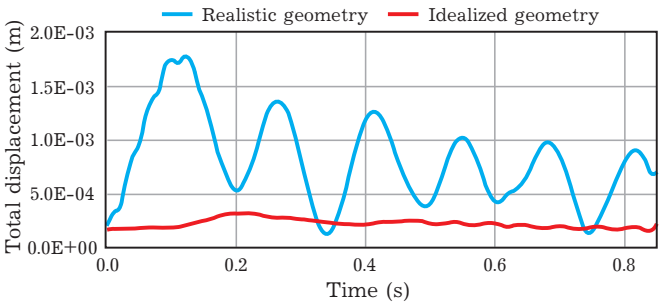

Fig. 5. Total displacement values of the plaque.

Figure 5 gives a comparison displaying the total volume displacement of the plaque. One can notice that the way the plaque is moving in the real geometry is totally different from that in the idealized one. The stenosis is symmetric in the idealized artery, on the other hand, in the real geometry, the total displacement is influenced by the volume flow rate in the common carotid artery which divides into the internal and external carotid branches.

The velocity magnitude plot shows approximately the same variations for both geometries after the inlet pressure's peak (see Figure 3) as shown in Figure 6, where those values are overestimated in the idealized case.

For the WSS (see Figure 7), as the observations made for the velocity magnitude, the variations are the same for both geometries after the inlet pressure's peak, since this hemodynamic indicator is the tangential stress that the fluid exerts on the wall, consisting on the tangential component of the stress tensor, which is given by $\boldsymbol{\sigma} = p\mathbf{I} - \boldsymbol{\tau}$, on the wall:

$$WSS = \boldsymbol{\sigma}_n - (\boldsymbol{\sigma}_n \cdot \mathbf{n})\mathbf{n} = \boldsymbol{\tau}_n - (\boldsymbol{\tau}_n \cdot \mathbf{n})\mathbf{n},$$

where $\mathbf{n}$ is the outward unit normal to the wall surface, and $\boldsymbol{\sigma}_n$ and $\boldsymbol{\tau}_n$ are the normal components of the stress and extra-stress tensors, respectively [24]. These overestimations observed for the velocity magnitude and the WSS values in the idealized case should be related to the geometries construction, and therefore to the position of the plaque, the flow rate, the displacement of the artery, etc.

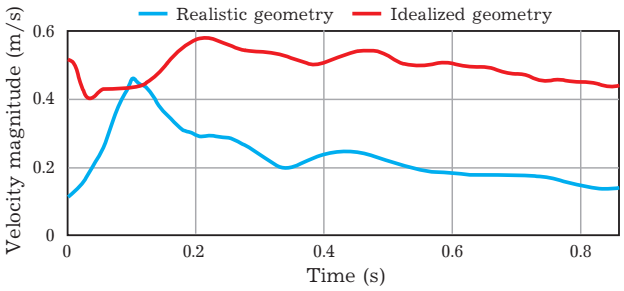

Fig. 6. Fluid velocity magnitude.

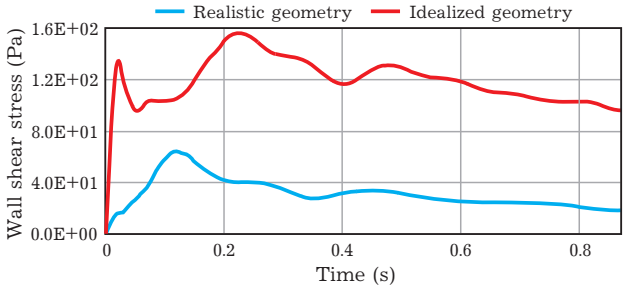

Fig. 7. WSS Maximal values distribution on the fibrous cap.

5. Conclusion

In summary, the FSI analysis performed in the models reveals that there is, qualitatively, good agreement among some hemodynamic indicators between idealized atherosclerotic artery and patient-specific atherosclerotic carotid artery geometries, indicating that the velocity magnitude and the WSS have the same variations after the pressure's peak but overestimating those values in the idealized case. These overestimations can be eliminated by implementing the same FSI numerical model in 3D idealized carotid bifurcation. We conclude that the idealized geometry used in this study can be used for accurate simulations of a patient-specific atherosclerotic carotid artery when the patient-specific geometry is not always available from the medical images.

[1] Ross R. Atherosclerosis — An inflammatory disease. New England Journal of Medicine. **340**, 115–126 (1999).

[2] Kayashima Y., Maeda-Smithies N. Atherosclerosis in Different Vascular Locations Unbiasedly Approached with Mouse Genetics. Genes. **11** (12), 1427 (2020).

[3] Chang Y. C., Hou T. Y., Merriman B., Osher S. A Level Set Formulation of Eulerian Interface Capturing Methods for Incompressible Fluid Flows. Journal of Computational Physics. **124** (2), 449–464 (1996).

[4] Peskin C. S. Numerical analysis of blood flow in the heart. Journal of Computational Physics. **25** (3), 220–252 (1977).

[5] Peskin C. S., McQueen D. M. A three-dimensional computational method for blood flow in the heart — I. Immersed elastic fibers in a viscous incompressible fluid. Journal of Computational Physics. **81** (2), 372–405 (1989).

[6] Glowinski R., Pan T.-W., Periaux J. A fictitious domain method for Dirichlet problem and applications. Computer Methods in Applied Mechanics and Engineering. **111** (3–4), 283–303 (1994).

[7] Glowinski R., Pan T.-W., Periaux J. A fictitious domain method for external incompressible viscous flow modeled by Navier–Stokes equations. Computer Methods in Applied Mechanics and Engineering. **112** (1–4), 133–148 (1994).

[8] Frei S., Richter T., Wick T. Eulerian Techniques for Fluid–Structure Interactions: Part II – Applications. In: Abdulle A., Deparis S., Kressner D., Nobile F., Picasso M. (eds) Numerical Mathematics and Advanced Applications – ENUMATH 2013. Lecture Notes in Computational Science and Engineering. **103**, 755–762 (2015).

[9] Wick T. Flapping and contact FSI computations with the fluid-solid interface-tracking/interface-capturing technique and mesh adaptivity. Computational Mechanics. **53**, 29–43 (2014).

[10] Hughes T. J. R., Liu W. K., Zimmermann T. K. Lagrangian–Eulerian finite element formulation for incompressible viscous flows. Computer Methods in Applied Mechanics and Engineering. **29** (3), 329–349 (1994).

[11] Donea J., Giuliani S., Halleux J. P. An arbitrary lagrangian-eulerian finite element method for transient dynamic fluid–structure interactions. Computer Methods in Applied Mechanics and Engineering. **33** (1–3), 689–723 (1982).

[12] Nobile F. Numerical Approximation of Fluid-Structure Interaction Problems with Application to Haemodynamics. Ph.D thesis; École Polytechnique Fédérale de Lausanne, Switzerland (2001).

[13] Boujena S., Kafi O., El Khatib N. A 2D mathematical model of blood flow and its interactions in the atherosclerotic artery. Mathematical Modelling of Natural Phenomena. **9** (6), 46–68 (2014).

[14] Boujena S., Kafi O., El Khatib N. Generalized Navier–Stokes equations with non-standard conditions for blood flow in atherosclerotic artery. Applicable Analysis. **95** (8), 1645–1670 (2016).

[15] El Khatib N., Kafi O., Tiago J., Sequeira A. Numerical simulations of a 3D fluid-structure interaction model for blood flow in an atherosclerotic artery. Mathematical Biosciences and Engineering. **14** (1), 179–193 (2017).

[16] El Khatib N., Génieys S., Volpert V. Atherosclerosis initiation modeled as an inflammatory process. Mathematical Modelling of Natural Phenomena. **2** (2), 126–141 (2007).

[17] El Khatib N. Modélisation mathématique de l'athérosclérose. Ph.D thesis; Université Claude Bernard–Lyon 1, France (2009).

[18] Faggiano E., Formaggia L., Antiga L. An open-source tool for patient-specific fluid-structure vessel mesh generation. Fifth International Symposium on Modelling of Physiological Flows, Chia Laguna, Italy (2013).

[19] Gambaruto A. M., Janela J., Moura A., Sequeira A. Sensitivity of hemodynamics in a patient specific cerebral aneurysm to vascular geometry and blood rheology. Mathematical Biosciences and Engineering. **8** (2), 409–423 (2011).

[20] Guerra T., Tiago J., Sequeira A. Optimal control in blood flow simulations. International Journal of Non-Linear Mechanics. **64**, 57–69 (2014).

[21] Ciarlet P. G. Mathematical Elasticity. Vol. 1. Three Dimensional Elasticity. North-Holland (1988).

[22] Janela J., Moura A., Sequeira A. Absorbing boundary conditions for a 3D non-Newtonian fluid-structure interaction model for blood flow in arteries. International Journal of Engineering Science. **48** (11), 1332–1349 (2010).

[23] Janela J., Moura A., Sequeira A. A 3D non-Newtonian fluid–structure interaction model for blood flow in arteries. Journal of Computational and Applied Mathematics. **234** (9), 2783–2791 (2010).

[24] Ramalho S., Moura A., Gambaruto A. M., Sequeira A. Sensitivity to outflow boundary conditions and level of geometry description for a cerebral aneurysm. International Journal for Numerical Methods in Biomedical Engineering. **28** (6–7), 697–713 (2012).

[25] Li Z.-Y., Howarth S., Trivedi R. A., U-King-Im J. M., Graves M. J., Brown A., Wang L., Gillard J. H. Stress analysis of carotid plaque rupture based on in vivo high resolution MRI. Journal of Biomechanics. **39** (14), 2611–2622 (2006).

[26] Tang D., Yang C., Zheng J., Woodard P. K., Sicard G. A., Saffitz J. E., Yuan C. 3D MRI-based multicomponent FSI models for atherosclerotic plaques. Annals of Biomedical Engineering. **32**, 947–960 (2004).

Чисельна тривимірна модель взаємодії рідини та структури кровотоку в атеросклеротичній сонній артерії

Кафі О.

CEMAT-Центр обчислювальної та стохастичної математики, Університет Лісабона, Авеню Ровіско Паіс 1049-001 Лісабон, Португалія

Переконливі докази показують зв'язок запалення з атеросклерозом, однією з головних причин смертності та захворюваності в усьому світі. Нещодавні дослідження показали, що запальний процес атеросклеротичних уражень бере участь у прогресуванні атеросклеротичних бляшок у певних областях, таких як біфуркація сонної артерії, які становлять ризик ішемічного інсульту в результаті взаємодії між кров'ю та бляшкою. Моделювання починається з використанням 3D-ідеалізованої геометрії, щоб зафіксувати найважливіші особливості таких взаємодій. Потім переходимо до частково специфічної для пацієнта обчислювальної області, що представляє атеросклеротичну артерію. Розуміння таких взаємодій є надзвичайно важливим для запобігання ризику розриву бляшки. Порівняння чисельних результатів показало, що якісно існує узгодженість між ідеалізованою атеросклеротичною артерією та специфічною для пацієнта атеросклеротичною сонною артерією. Ідеалізована геометрія сонної артерії буде корисною в майбутніх дослідженнях гемодинамічних показників FSI на основі медичних зображень.

Ключові слова: *атеросклероз; кровотік; біфуркація сонної артерії; взаємодія рідина–структура (FSI).*